On the relation between tree crown morphology and particulate matter deposition on urban tree leaves: A ground-based LiDAR approach

On the relation between tree crown morphology and particulate matter deposition on urban tree leaves: a ground-based LiDAR approach.

Jelle Hofman[1], Harm Bartholomeus[2], Kim Calders[2], Shari Van Wittenberghe[1], Karen Wuyts[1], Roeland Samson[1]

[1] Laboratory of Environmental and Urban Ecology, University of Antwerp, 2020 Antwerp, Belgium
[2] Laboratory of Geo-Information Science and Remote Sensing, Wageningen University, Droevendaalsesteeg 3, Wageningen 6708 PB, The Netherlands

Corresponding Author:

Jelle Hofman
Postal Address: University of Antwerp, Department of Bioscience Engineering, Groenenborgerlaan 171, 2020 Antwerp, Belgium
Tel. +32 (0)3 265 35 69
Fax. +32 (0)3 265 32 25
E-mail Address: Jelle.Hofman@uantwerpen.be

Keywords:

Particulate matter; Urban green; Light detection and ranging (LiDAR); Leaf-deposition; Tree morphology

Abstract

Urban dwellers often breathe air that does not meet the European and WHO standards. Next to legislative initiatives to lower atmospheric pollutants, much research has been conducted on the potential of urban trees as mitigation tool for atmospheric particles. While leaf-deposited dust has shown to vary significantly throughout single tree crowns, this study evaluated the influence of micro-scale tree crown morphology (leaf density) on the amount of leaf-deposited dust. Using a ground-based LiDAR approach, the three-dimensional tree crown morphology was obtained and compared to gravimetric measurements of leaf-deposited dust within three different size fractions (>10, 3-10 and 0.2-3µm). To our knowledge, this is the first application of ground-based LiDAR for comparison with gravimetric results of leaf-deposited particulate matter. Overall, an increasing leaf density appears to reduce leaf-deposition of atmospheric particles. This might be explained by a reduced wind velocity,

suppressing turbulent deposition of atmospheric particles through impaction. Nevertheless, the effect of tree crown morphology on particulate deposition appears almost negligible (7% AIC decrease) compared to the influence of physical factors like height, azimuth and tree position.

1. Introduction

Despite emission reductions of the main air pollutants in the last decade, air pollution still poses an important threat to public health, the economy and the ecosystems we depend on (EEA 2013, WHO 2014). The impacts of air pollution are most strongly felt in urban areas, which currently accommodate over 50% of the global population (WHO 2010) and in ecosystems, where the pressures of air pollution impairs vegetation growth and harms biodiversity (EEA 2013). In terms of potential harm to human health, particulate matter (PM) poses the greatest risk, as it penetrates into sensitive regions of the respiratory system and can lead to severe health effects and premature mortality (EEA 2013). While scientific evidence does not suggest any threshold below which no adverse health effects would be expected when exposed to PM (WHO 2006), currently more than 85% of the EU's urban population is exposed to PM levels above the 2005 WHO Air Quality Guidelines (EEA 2013). Moreover, it can be expected that the impact of urban air pollution will only increase further as 70% of the global population will live in cities by 2050 (WHO 2010).

Source regulations at multiple constitutional levels are indispensable to reduce the cross-boundary impact of air pollution. Nevertheless, growing interest has increased the need for exposure measures that influence atmospheric pollutant concentrations by stimulation of deposition and/or dispersion processes. In this context, research has been conducted on the potential role of urban vegetation as a mitigation tool for atmospheric particulate matter (Beckett et al. 1998, 2000, Yang et al. 2005, Langner 2007, Litschke and Kuttler 2008, Sæbø et al. 2012, Maher et al. 2013). Because of its high leaf area relative to the ground area it covers, vegetation (especially trees) can influence local atmospheric particle concentrations both directly, by deposition on its surfaces (Ruijgrok et al. 1997, Sæbø et al. 2012, Terzaghi et al. 2013, Hofman et al. 2014a), and indirectly, by influencing dispersion of PM

polluted air (Gromke and Ruck 2007, Langner 2007, Vos et al. 2013). Previous research reported on the variation of leaf-deposited dust within single tree crowns and the influence of physical factors like sampling height, wind and street canyon ventilation on the observed variation in dust deposition (Langner 2007, Hofman et al. 2013, Hofman et al. 2014a). This study focusses on variation in leaf-deposited particle mass by evaluating the potential influence of tree crown morphology. Both dispersion and deposition of atmospheric particles are namely influenced by the boundary layer thickness of the air close to the object. Surface roughness increases the boundary layer thickness, hence the momentum of mass transport between the air and the object.

In this study, we tried to establish a relation between the micro scale leaf density of the tree crown, obtained by detailed ground-based Light Detection and Ranging (LiDAR) measurements, and the weight of leaf-deposited particles within three different size fractions, namely large (>10 μm), coarse (3-10 μm) and fine (0.2-3 μm) particles. The influence of leaf density was tested for two scenarios with respect to the considered leaf sampling locations. We tested for an aerodynamic effect of the surrounding canopy (scenario 1) and the wash-off effect of the upper canopy (scenario 2). In scenario 1, we expect a dense surrounding canopy to reduce wind speed resulting in lower deposition rates as the process of turbulent deposition through impaction is weakened (Lee and Mukund 1993, Litschke and Kuttler 2008, Steffens et al. 2012). For scenario 2, we hypothesize that a dense upper canopy might lead to increased wet deposition at the sampling location due to particle wash-off from the upper canopy layers (Urbat et al. 2004, Zhang et al. 2006, Mitchell et al. 2010). To evaluate these scenarios, we quantified the amount of leaf surface-deposited particles gravimetrically within three different size fractions (0.2-3 μm, 3-10 μm and >10 μm) at 72 positions within six urban tree crowns, situated in a street canyon. A LiDAR analysis was conducted to obtain detailed information on the three-dimensional tree crown morphology.

2. Material and Methods

A typical urban street canyon was selected in the densely populated city center of Antwerp, Belgium (51°11'45.75"N, 4°25'26.46"E; Figure 1). The street canyon consists of two opposing traffic lanes separated by a row of London plane (*Platanus x acerifolia* Willd.) trees and has a typical street canyon geometry with a width (W) of 15 m, a length (L) of 90 m and a height (H) of 10 m. According to the geometry rules described by Vardoulakis et al. (2003), the street canyon can thus be described as a long (L/H>7) regular street canyon (aspect ratio (H/W)<1). The street is characterised by six densely foliated plane trees (T1-T6) with tree crowns reaching from a height of about 4 m (onset of the crown) to 15 m (top of the crown). While the street itself is relatively quiet in terms of traffic (50 vehicles h^{-1} (SGS 2010)), it is located in the vicinity (200 and 400 m) of two busy thoroughfares of Antwerp (*Binnensingel* and *R1*), as can be seen on Figure 1.

Figure 1: Location of the street canyon with the considered tree crowns (T1-T6) in Antwerp (left, source: Google) and a 3D visualisation of the street canyon based on the LiDAR data (right).

2.1 Quantification of leaf-deposited particulate matter

A leaf sampling campaign was conducted at the end of the growing season, on September 10 and 11, 2012, in order to optimise magnetic differentiation between the sampling locations. Previous studies, namely, reported on continuous leaf surface particle accumulation throughout the in-leaf season (Kardel et al. 2011, Hofman et al. 2014b). The urban tree crowns were sampled using a boom lift at three heights (3.5, 8.5 and 13.5 m) and four azimuthal directions (NE, NW, SE, SW) around the tree crowns. At each of the 72 sampling locations, three samples were collected, with each sample consisting of five fully developed and undamaged leaves. These leaf samples were placed in paper bags, labelled and transported to the laboratory for analysis.

Laboratory analyses were carried out at the Bioscience Engineering Department and the Laboratory for Bio-organic Mass Spectroscopy of the Department of Pharmaceutical Sciences at the University of Antwerp, Belgium. At the laboratory, each collected leaf sample consisting of five leaves was hand washed using nitrile powder free disposable gloves (VWR International) in 800 ml ultrapure water (<0.1 µs cm^{-1}) (Eurowater, Belgium). The washed leaf area was determined using a Li-3100 area meter (LI-COR Environmental, US). Subsequently, the washing water was stored in an acclimatised dark room at 16°C awaiting filtration. For the filtration procedure, we used Nuclepore track-etched polycarbonate filter membranes (Whatman, UK). These filter membranes were pre-weighed after 24 hour equilibration time at 50% relative humidity (to stabilise the humidity of the hygroscopic filters). Filter mass was determined using a 1 µg precision Mettler MT5 balance (Mettler-Toledo International Inc., Switzerland). To avoid electrostatic charges on the filters, they were passed through an ionizer antistatic system (Mettler-Toledo International Inc., Switzerland) before weighing. Following pre-weighing, the filter membranes were transported to the laboratory in labelled petrislide dishes (Millipore Corp., US) awaiting filtration. The day of filtration analysis, the washing water was shaken up for 4 hours at a rotation frequency of 150 rpm using a KS 260 basic shaker (IKA-WERKE GMBH & CO.KG, Germany) in order to resuspend all washed particles. To avoid filter membrane saturation, only

100 ml of the shaken washing water was filtered, using a 47 mm glass filter funnel (GE Healthcare, UK) connected to a vacuum pump (GE Healthcare, UK), over the pre-weighed filter membranes with pore sizes of in succession 10, 3 and 0.2 µm. For the 0.2 µm pore size, we used two filter membranes to avoid filter membrane saturation. Doing so, we collected three size fractions of surface-deposited particulate matter on the filters: large (>10 µm), coarse (3-10 µm) and fine (0.2-3 µm). Loaded filters were subsequently dried at ambient temperature, equilibrated for 24 hours at 50% relative humidity and post-weighed to calculate the resulting leaf-deposited particulate mass in every size fraction of each washed leaf sample (post- minus pre-weight). A potential influence of the applied procedure was evaluated for every size fraction by completing the entire filtration procedure using only ultrapure water on pre-weighed filters (blanco). This blanco weight (post- minus pre-weight) was subtracted from the netto weight of the loaded filters (post- minus pre-weight). The resulting weight was finally normalized for filtered volume and washed leaf area. Doing so, we obtained the surface-deposited particle weight of each washed leaf sample within the different considered size fractions (0.2-3, 3-10 and >10 µm). Following this protocol, a total of 1080 leaves were washed and filtered over 648 filters. In the end we thus obtained the weight per leaf area (mg m^{-2}) of the leaf surface-accumulated particles (collected by washing) within the three different size fractions. The "total weight per leaf area" (in mg m^{-2}) was defined as the sum of all individual size fractions. The followed procedure and detailed analysis of the obtained results is presented in Hofman et al. (2014a).

Mean meteorological parameters were calculated from measurements conducted during the exposed in-leaf period from May 1 until September 11 at a monitoring station of the Flemish Environment Agency (VMM), located at 7 km from the considered Plane trees. During the in-leaf period, a mean temperature of 16°C, relative humidity of 73% and vector averaged wind direction and speed of respectively 227° and 1.40 m s^{-1} were obtained.

2.2 Three-dimensional description of tree crown structure

Ground-based Light Detection And Ranging (LiDAR) is an active remote sensing technology which provides a novel tool for generating a comprehensive and detailed 3D mathematical description of tree and canopy structure in a non-destructive manner (Van der Zande 2008). These state of the art systems are mobile, robust and small and can be used for diverse applications, e.g. airborne topographic mapping, surveying of buildings and plants, etc. (Van der Zande 2008).

In this study we used the RIEGL VZ-400 ground-based scanner (RIEGL Laser Measurement Systems GmbH, Austria). This time-of-flight scanner has a range up to 350 m and a beam divergence of nominally 0.35 mrad and operates in the near infrared (wavelength 1550 nm). The RIEGL VZ-400 scanner records multiple returns (up to four returns per emitted pulse), with returns being derived from onboard waveform processing. Multiple returns will lead to an improved sampling at greater canopy heights, which is of interest for monitoring vegetation (Lovell et al. 2003, Calders et al. 2014). The angular resolution in both zenith and azimuth direction was set to 0.06 degrees.

LiDAR data were acquired from all six trees and prior to the leaf sampling campaign, on September 7, 2012, to avoid potential effects of structural tree crown damage during the leaf sampling campaign. We used multiple scan locations and reflecting targets were distributed throughout the scene. These targets were used to register the individual scan locations to a single registered point cloud with the RiSCAN PRO software (provided by RIEGL). The points belonging to the individual trees were manually selected from the pointcloud. Next, these subsets were filtered, where all individual points that had a distance of ≥ 0.1 m to all other points were removed in order to remove noise. Further, due to the setup of the different scan locations some parts of the trees may be oversampled (e.g. due to overlapping scans and shorter distance to the scanner). Therefore, the pointclouds were converted to voxels (three-dimensional cell volumes) of 25 cm^3, where a voxel is considered filled if it contains a return.

To compare the PM measurements to the LiDAR data, we defined subsets of the voxelized trees at the leaf sampling locations (n=72). At each sampling location, different subset sizes and scenarios (see Figure 2) were used to test for the hypotheses outlined in the introduction. To test for the effect of tree crown structure on aerodynamic induced leaf deposition (scenario 1), we defined subsets with increasing volume (1, 3.375, 8 and 27 m^3) around the sampling location. Further, to evaluate the effect of tree crown structure on the wash-off induced leaf-deposition (scenario 2), we defined subsets with increasing voxel height (1, 1.5, 2 and 3 m^3) above the sampling location (Figure 2).

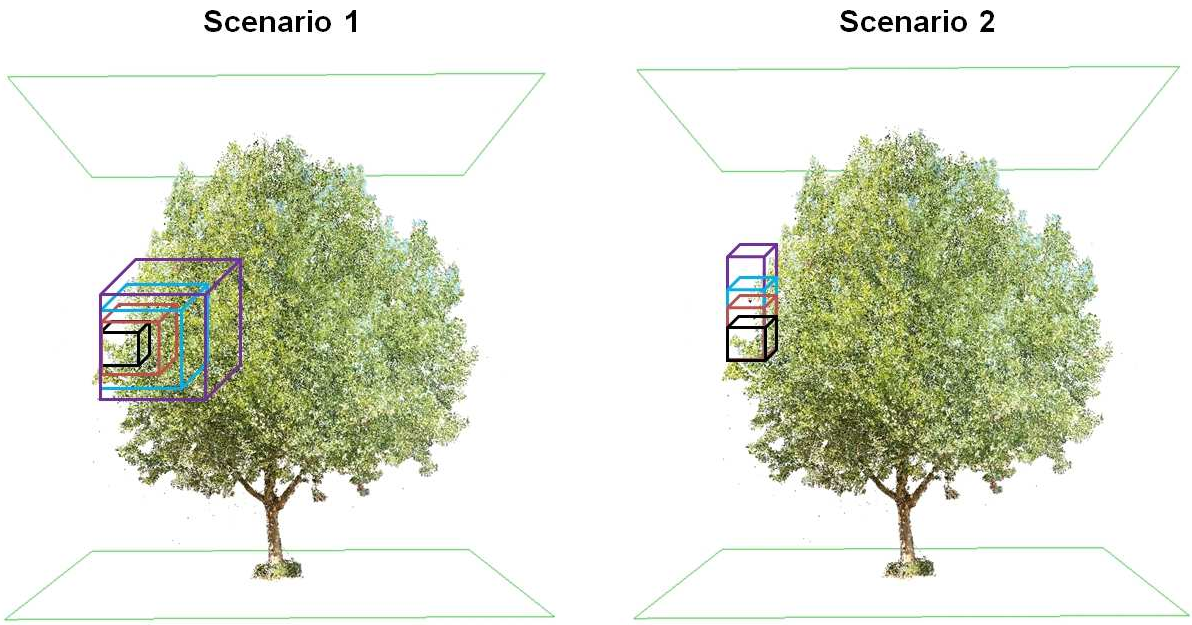

Figure 2: Schematic overview of the selected subsets for the considered scenarios. The increasing subset size (black-red-blue-purple) is shown for scenario 1 (1, 3.375, 8 and 27m^3) and 2 (1, 1.5, 2 and 3m^3).

For each sampling position (n=72), scenario (n=2) and subset size (n=4), the number of filled voxels per subset was obtained. From these numbers, we calculated the fraction of filled voxels (25 cm^3) per subset size (e.g. 1 m^3), which approximates the amount of leaf material inside each subset, and is hereafter referred to as "leaf density". Theoretically, it is also possible to derive the leaf area density (LAD) from the fraction of filled LiDAR voxels using the approach of Hosoi and Omasa (2006), but then additional information on the leaf inclination and the number of laser beams per voxel is required which is difficult to assess when multiple laser scans are combined. In order to avoid uncertainty

increases due to approximations, we, therefore, used the fraction of filled voxels per subset size (leaf density) instead of the LAD.

2.3 Statistical Analysis

Normality assumptions of the weight and LiDAR results were evaluated both visually (histogram and quantile-quantile plots) and statistically using the Shapiro-Wilk normality test. After logarithmic transformation of the LiDAR results, the spatial variation of both the number of LiDAR hits and the resulting leaf density throughout the street canyon was evaluated using linear mixed-effects models with the nlme package (Pinheiro et al. 2012) in R 2.15.2 software (R Core Team 2012). To cope with the nested design and the occurrence of both random and fixed effects, linear mixed-effects models were applied to test for the spatial variation of the LiDAR results using *height* (3.5, 8.5 and 13.5 m), *azimuth* (SE, SW, NW, NE) and *subset size* (1, 3.375, 8 and 27 m^3 for scenario 1 and 1, 1.5, 2 and 3 m^3 for scenario 2) as fixed factors and *azimuth* nested in *tree* as random factors.

Potential relations between leaf density and leaf-deposited particle weight were evaluated using regression and linear mixed-effects model analyses. To do so, a basic model was defined in which the leaf-deposited particle weight was explained by solely the physical factors, namely *height*, *azimuth* and *tree position* as fixed factors and *tree* as random factor. This model already showed to be representative for the same data set in Hofman et al. (2014a). Consequently, we included leaf density as a fixed factor inside this model. ANOVA analysis of models with and without leaf density revealed whether leaf density explained any additional variation. For each model, both bottom up and top down approaches were used in order to identify the best available model explaining the measurements using the Akaike information criterion (AIC).

Finally, possible non-linear relations between leaf density and leaf-deposited particle weight were evaluated using two-layer feed-forward neural networks in Matlab 8.1 software (MathWorks Inc. 2013). We defined nine neural networks (see Table 1) in which the total leaf-deposited particle weight was explained by *height*, *azimuth*, *tree*, *tree position* and the *leaf density* of the different subset sizes

and scenarios. While *height* was included as a continuous variable, categorical variables (*azimuth*, *tree*, *tree position*) were transformed into discrete numbers of potential states (Wang et al. 2008). This resulted in 14 input samples and 1 output sample. Each neural network consisted of 10 nodes and 60% of the total data (n=114) was used to train the network while 20% was used as validation data (n=38) and another 20% as test data (n=38). The Levenberg-Marquardt backpropagation algorithm (Hagan and Menhaj 1994, Lera and Pinzolas 2002) was used to train the networks. Training of a network stops when generalization stops improving, as indicated by an increase in the mean square error of the validation data. Each network (Table 1) was trained 20 times, including a network with randomly generated data, to be able to distinguish genuine relationships from statistical effects. The correlation coefficient (R) accounting for the goodness-of-fit between the measured and the modelled total weight and the RMSE indicating the association of each neural network were used to evaluate the potential of LiDAR data in explaining additional leaf-deposited particle weight variation.

Table 1: Input and output variables for the different considered neural networks (1-9).

Network	Input (n=190)	Output (n=190)	Number of nodes
1	Height (m), Azimuth (NE,NW,SW,SE), Tree (T1-T6), Tree position (edge-canyon)	Total Weight (mg m^{-2})	10
2	Height (m), Azimuth (NE,NW,SW,SE), Tree (T1-T6), Tree position (edge-canyon), LiDAR scenario 1-1m^3	Total Weight (mg m^{-2})	10
3	Height (m), Azimuth (NE,NW,SW,SE), Tree (T1-T6), Tree position (edge-canyon), LiDAR scenario 1-3.375m^3	Total Weight (mg m^{-2})	10
4	Height (m), Azimuth (NE,NW,SW,SE), Tree (T1-T6), Tree position (edge-canyon), Tree, LiDAR scenario 1-8m^3	Total Weight (mg m^{-2})	10
5	Height (m), Azimuth (NE,NW,SW,SE), Tree (T1-T6), Tree position (edge-canyon), Tree, LiDAR scenario 1-27m^3	Total Weight (mg m^{-2})	10
6	Height (m), Azimuth (NE,NW,SW,SE), Tree (T1-T6), Tree position (edge-canyon), Tree, LiDAR scenario 2-1m^3	Total Weight (mg m^{-2})	10
7	Height (m), Azimuth (NE,NW,SW,SE), Tree (T1-T6), Tree position (edge-canyon), LiDAR scenario 2-1.5m^3	Total Weight (mg m^{-2})	10
8	Height (m), Azimuth (NE,NW,SW,SE), Tree (T1-T6), Tree position (edge-canyon), Tree, LiDAR scenario 2-2m^3	Total Weight (mg m^{-2})	10
9	Height (m), Azimuth (NE,NW,SW,SE), Tree (T1-T6), Tree position (edge-canyon), Tree, LiDAR scenario 2-3m^3	Total Weight (mg m^{-2})	10
Random	Random data sets (14)	Total Weight (mg m^{-2})	10

3. Results and Discussion

The quantified average leaf-deposited particle weight per unit leaf area was 38, 34 and 676 mg m^{-2} for the 0.2-3, 3-10 and >10 µm size fraction, respectively. The total particle mass (sum of all size fractions) was dominated by the >10 µm fraction (90% of the total particle mass), followed by significantly smaller contributions of the 3-10 µm and the 0.2-3 µm size fractions (4.5% and 5% respectively). A

detailed analysis of the obtained leaf-deposited weight results can be found in Hofman et al. (2014a). The LiDAR results ranged from a minimum of 20 filled voxels (leaf density of 0.25%) to a maximum of 39057 filled voxels (leaf density of 18%) considering the different subset sizes for scenario 1 and 5799 voxels (leaf density of 24%) for the subset sizes in scenario 2 (Table 2). Leaf density ranged from a minimum of 0.25% (20 filled voxels) to a maximum of 31% (2502 voxels in the smallest subset size) for both scenario 1 and 2.

Table 2: Average, minimum (min) and maximum (max) number of filled voxels (#) and leaf density (%) for the different subset sizes of the considered scenarios.

Scenario 1								
Subset size	*1 m³*		*3.375 m³*		*8 m³*		*27 m³*	
	Filled Voxels (#)	Leaf density (%)	Filled Voxels (#)	Leaf density (%)	Filled Voxels (#)	Leaf density (%)	Filled Voxels (#)	Leaf density (%)
Average	722.25	9.03	2413.18	8.94	5486.12	8.57	17072.61	7.90
Min	20	0.25	285	1.06	883	1.38	2124	0.98
Max	2502	31.27	6137	22.73	13288	20.76	39057	18.08
Scenario 2								
Subset size	*1 m³*		*1.5 m³*		*2 m³*		*3 m³*	
	Filled Voxels (#)	Leaf density (%)	Filled Voxels (#)	Leaf density (%)	Filled Voxels (#)	Leaf density (%)	Filled Voxels (#)	Leaf density (%)
Average	722.25	9.03	1097.95	9.15	1462.44	9.14	2207.04	9.20
Min	20	0.25	132	1.10	214	1.34	298	1.24
Max	2502	31.27	3619	30.16	4657	29.11	5799	24.16

3.1 Spatial variation of the number of filled voxels and leaf density

Evaluating the spatial variation of the tree crown morphology, linear mixed-effects models of the LiDAR results reveal the highest leaf density at the middle height of the tree crowns, both for the number of filled voxels ($p<0.0001$) and leaf density ($p<0.0001$) (Table 3). These results agree with former studies reporting on LAD distributions for different tree species along a vertical gradient (Èermák 1998, Hosoi and Omasa 2006, Hosoi and Omasa 2007, Zande et al. 2008). Next to the effect of height, the lowest leaf density can be found at the NW azimuth (shadow side) as shown by both the number of voxels ($p=0.04$ and $p=0.003$) and leaf density ($p=0.002$ and $p=0.003$) for scenario 1 and 2, respectively. For the leaf density of scenario 1, a 17 % decrease can be observed at the NW azimuth (7.13 %) with regard

to the average leaf density of all azimuthal directions (8.61 %). The azimuth effect weakens near the middle height of the tree crowns as suggested by the *height:azimuth* interactions (Table 3). To our knowledge, azimuthal effects on LAD distribution have not yet been reported. Nevertheless, the observed azimuthal leaf density differences might be a strategy of the tree crowns in order to intercept maximal solar irradiance. As can be expected, increasing the subset size for respectively scenario 1 (1-3.375-8-27 m^3) and scenario 2 (1-1.5-2-3 m^3) yields significantly more filled voxels ($p<0.0001$ and <0.0001) while the average leaf density remains unchanged (8.6% and 9.1%).

Table 3: Linear mixed-effects model results of height, azimuth, subset size and their interactions on the number of filled voxels and the resulting leaf density for scenario 1 (upper) and scenario 2 (lower). Significant effects (p<0.05) are shown in bold.

	Scenario 1 (n=288)							
	Number of filled voxels				*Leaf density*			
	numDF	denDF	F-value	p-value	numDF	denDF	F-value	p-value
Intercept	**1**	**270**	**7.212**	**<0.0001**	**1**	**270**	**837.5337**	**<0.0001**
Height	**2**	**270**	**21.735**	**<0.0001**	**2**	**270**	**37.9474**	**<0.0001**
Azimuth	**3**	**270**	**2.939**	**0.0355**	**3**	**270**	**5.1307**	**0.0018**
Subset size	**1**	**270**	**463.52**	**<0.0001**	1	270	0.009	0.9245
Height:Azimuth	6	270	1.624	0.1405	**6**	**270**	**2.8352**	**0.0108**
	Scenario 2 (n=288)							
	Number of filled voxels				*Leaf density*			
	numDF	denDF	F-value	p-value	numDF	denDF	F-value	p-value
Intercept	**1**	**270**	**3.189**	**<0.0001**	**1**	**270**	**469.3578**	**<0.0001**
Height	**2**	**270**	**15.438**	**<0.0001**	**2**	**270**	**15.8107**	**<0.0001**
Azimuth	**3**	**270**	**4.731**	**0.0031**	**3**	**270**	**4.8449**	**0.0027**
Subset size	**1**	**270**	**150.502**	**<0.0001**	**1**	**270**	**4.1554**	**0.0425**
Height:Azimuth	**6**	**270**	**3.817**	**0.0011**	**6**	**270**	**3.909**	**0.0009**

3.2 Linear relation between leaf density and leaf-deposited particle weight

We first tested for the direct relation between leaf density and the leaf-deposited weight by fitting regression lines of both variables (n=190). For scenario 1 (Figure 3), no significant association is obtained for the total weight ($0.005<R^2<0.023$), neither the individual size fractions ($0.016<R^2<0.023$ for 0.2-3 µm; $0.01<R^2<0.03$ for 3-10 µm and $0.004<R^2<0.020$ for >10 µm). Nevertheless, a negative

slope is suggested by all 16 trendlines (Figure 3). Best association is obtained between a subset size of 8 m³ and the weight of the 3-10 µm size fraction. Comparable trends and associations (R^2) are obtained when the voxel numbers are plotted against the leaf-deposited particle weight (not shown).

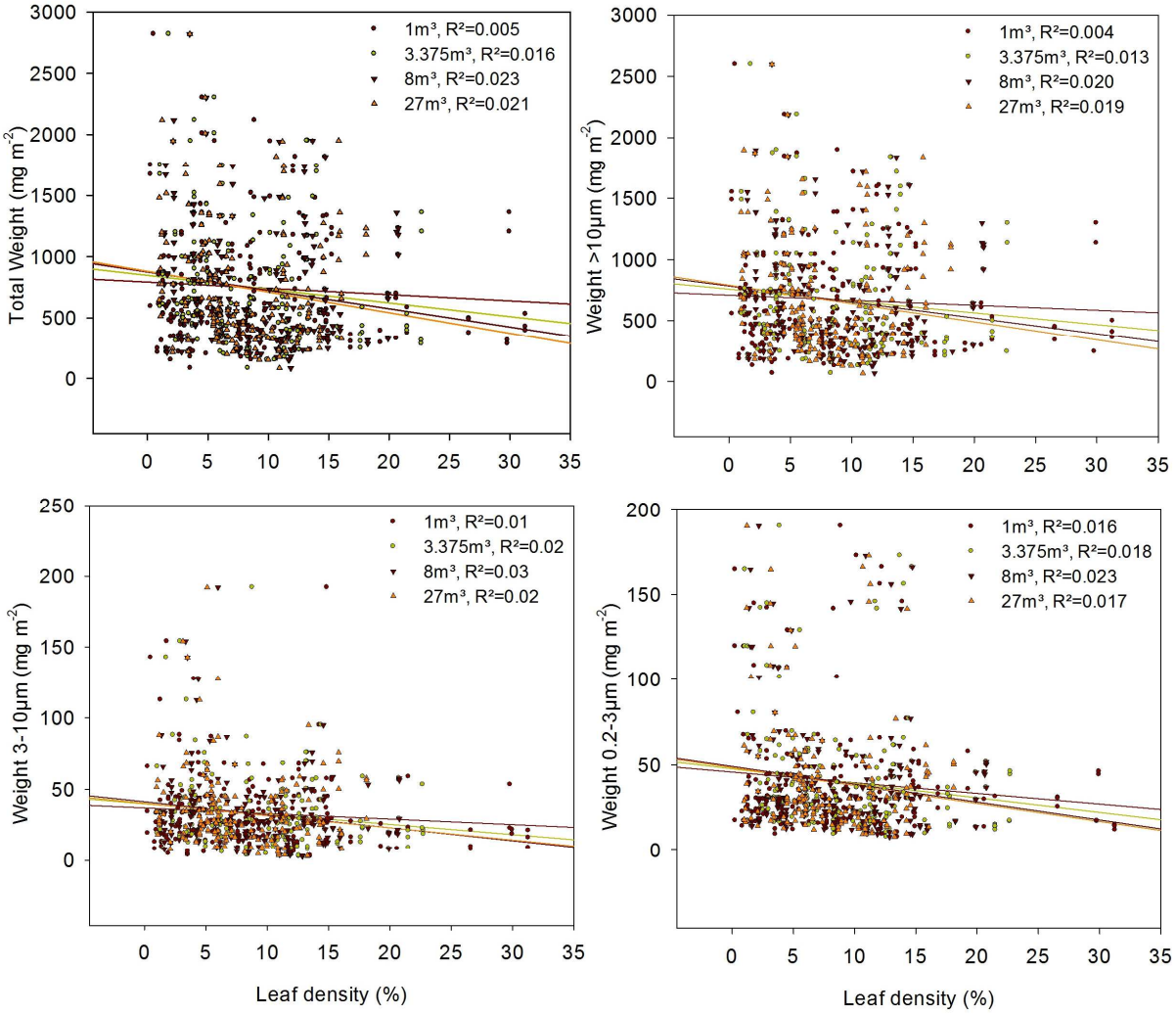

Figure 3: Relation of leaf density with leaf-deposited particle weight (mg m^{-2}) for the different subset sizes (1, 3.375, 8 and 27 m³) of scenario 1 within the total (upper left), >10 µm (upper right), 3-10 µm (lower left) and 0.2-3 µm (lower right) particle size fractions.

Weak associations are also obtained for scenario 2 (Figure 4) for both total weight ($0.0005<R^2<0.005$) and weight of the individual particle size fractions ($0.009<R^2<0.016$ for 0.2-3 µm; $0.002<R^2<0.011$ for 3-10 µm and $0.0002<R^2<0.004$ for >10 µm). A negative linear trend is suggested with increasing slope as the subset size increases (Figure 4). Best association is obtained for the smallest subset size (1 m³)

and the weight of the smallest size fraction (0.2-3 µm). Comparable trends and associations (R^2) are obtained when the voxel numbers are plotted against the leaf-deposited particle weight (not shown). As identical trends and associations are observed for the number of voxels as for leaf density, we restricted to the evaluation of the effect of leaf density in the further linear mixed-effects model and neural network analyses.

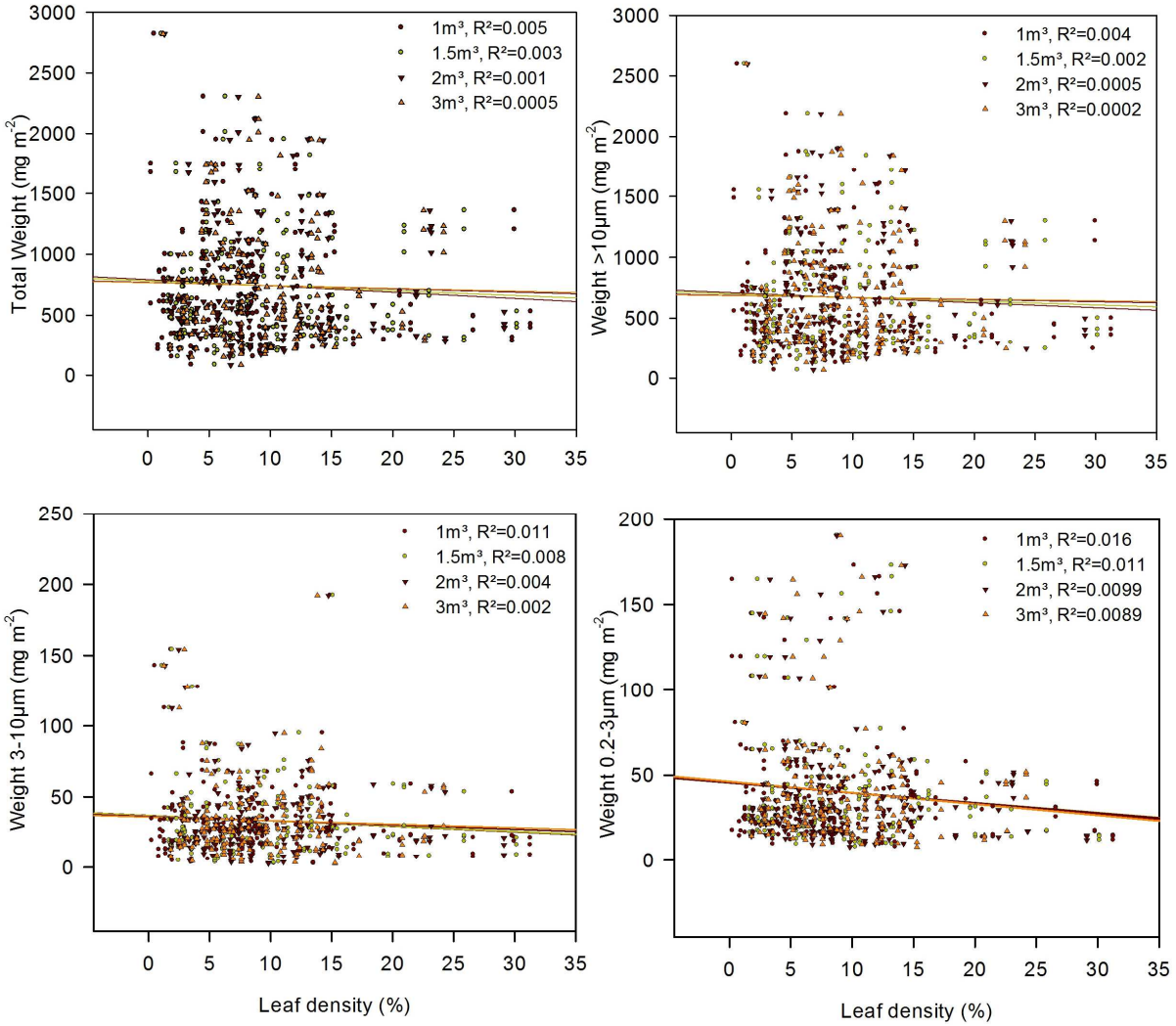

Figure 4: Relation of the leaf density with the leaf-deposited particle weight (mg m^{-2}) for the different subset sizes (1, 1.5, 2 and 3m^3) of scenario 2 within the total (upper left), >10µm (upper right), 3-10µm (lower left) and 0.2-3µm (lower right) particle size fractions.

Part of the spatial variation of the leaf-deposited particle mass inside the tree crowns is influenced by physical factors as was previously shown by significant *height*, *azimuth* and *height:tree position* effects

of the same data (leaf-deposited particle mass) in a recent study of Hofman et al. (2014a). Decreased leaf-deposited particle weight with height was observed, probably due to the distance to the emission source and potential wash-off at the top of the canopy, and a wind-induced distribution of atmospheric particles showed to result in highest leaf-deposits at the downwind (NE) tree crown locations (Hofman et al. 2014a). Because of these physical effects, we tested whether leaf density was able to explain part of the residual variation by including it as a fixed factor within the linear mixed-effects model of the physical effects. ANOVA analysis was conducted to test whether the extensive model (with leaf density) was able to explain more variation than the model with solely the physical effects using the AIC criterion. Results of this analysis are shown in Table 4.

For the total leaf-deposited weight (sum of all size fractions), the 0.2-3 and >10 µm size fraction, the extensive models (model 2-9) explained significantly more variation than the model with solely physical effects (model 1) except for model 7 ($p=0.32$), as can be seen in Table 4. As hypothesized for scenario 1, increasing leaf density results in a decreasing leaf-deposited particle mass per unit leaf area. But this effect is only significant at the NW ($p=0.0002$) and SE ($p=0.002$) azimuth, as indicated by significant *azimuth*:*leaf density* interactions ($p<0.01$) for all scenario 1 models (model 2-5). Compared with the wind field distribution throughout the considered exposure period (Figure 5), these azimuths seem to coincide with the leaf sampling locations in the middle of the street canyon. At these locations, the effect of wind will be most strongly felt, as the street canyon morphology will shelter the tree crowns from free air flow near the street canyon walls. In the study of Hofman et al. (2014a), this was evidenced by higher leaf deposits at the downwind (NE) locations, due to a concentration of particles at the downwind street canyon wall. Due to the relatively low wind speed (1.40 m s^{-1}, see 2.1) and the street canyon morphology (H/W<1), formation of a canyon vortex (Vardoulakis et al. 2003, Gromke and Ruck 2007) can be ruled out.

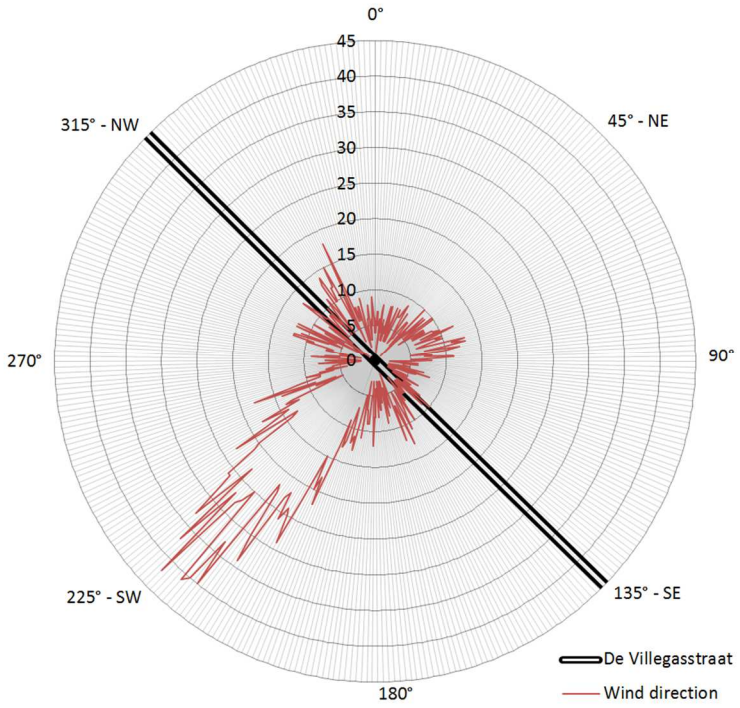

Figure 5: Polar plot of hourly wind directions (°) between May and September 11th 2012 (data source: VMM) from Hofman et al. (2014a).

Decreasing leaf-deposited particle weight with increasing leaf density was observed for scenario 2 as well. This contradicts our hypothesis of wet deposition of rain-induced wash-off from higher positioned leaves. As the smallest subset size (1m³) of scenario 2 explains most variation (Table 4), we can assume that the density of the upper canopy layers does not influence the amount of leaf-deposited dust on lower positioned leaves. Based on our data, no quantifiable effect of particle wash-off off from the upper canopy layers can thus be observed. Contrasting results of rain-induced particle wash-off have been reported. While some studies found a major effect of precipitation on the seasonal accumulation of magnetisable leaf-deposited particles (Matzka and Maher 1999, Zhang et al. 2006, Mitchell et al. 2010), other studies argue that the effect of rain is very limited (Urbat et al. 2004, Szönyi et al. 2008, Kardel et al. 2011). A previous biomonitoring study of Hofman et al. (2014b), on the same tree species (*Platanus x acerifolia* Willd.) as applied in this study, showed no effect of rain induced wash-off on the leaf surface accumulation of magnetisable particles. Based on the AIC criterion, we can say that the 3.375 m³ subset size of scenario 1 (model 3) explains most leaf-deposited weight variation.

Nevertheless, it only accounts for a 7% decrease of the AIC criterion, compared to the model with solely physical effects (model 1).

Table 4: ANOVA results in order to compare between the linear mixed-model analysis of the leaf-deposited particle weight by physical effects (height, azimuth and tree position: model 1) and the extensive linear mixed-effects models which include leaf density at different subset sizes of the considered scenarios (model 2-9).

Model	Effects	df	AIC	BIC	p-value
Model 1	Physical effects	9	252.31	281.54	
Model 2	Physical effects + LiDAR scenario 1: 1m³	14	237.26	282.72	<0.0001
Model 3	Physical effects + LiDAR scenario 1: 3.375m³	15	234.33	283.04	<0.0001
Model 4	Physical effects + LiDAR scenario 1: 8m³	11	237.25	272.97	<0.0001
Model 5	Physical effects + LiDAR scenario 1: 27m³	17	239.89	295.09	<0.0001
Model 6	Physical effects + LiDAR scenario 2: 1m³	14	247.96	293.42	0.0135
Model 7	Physical effects + LiDAR scenario 2: 1.5m³	10	253.32	285.79	0.32
Model 8	Physical effects + LiDAR scenario 2: 2m³	9	250.2	279.43	-
Model 9	Physical effects + LiDAR scenario 2: 3m³	13	248.12	290.33	0.016

3.3 Non-linear relation between leaf density and leaf-deposited particle weight

Possible non-linear effects of leaf density on the leaf-deposited particle mass were evaluated using neural networks in Matlab (see 2.3). The correlation coefficient (R) accounting for the association between the measured and the modelled total weight and the RMSE indicating the coincidence of each network are presented in Table 5. From ANOVA analysis of the correlation and RMSE results, it appears that all networks differ significantly from the network based on random data. Network 1, which uses only physical effects (*height*, *azimuth*, *tree position* and *tree number*) to explain the obtained weight results, yields significantly better average association ($r=0.56$, $p<0.0001$) and average coincidence (RMSE=420.72 mg m^{-2}) compared to the network based on random data ($r=0.03$, RMSE=548.98 mg m^{-2}). Network 2 to 9, where leaf density was included as an explaining variable, all show significantly higher associations and coincidences compared to the random dataset, but do not differ from the network where only physical effects were included (Figure 6).

Since network 1 yields the best correlations and the lowest RMSEs (Figure 6, Table 5), no beneficial effect of including leaf density in the neural networks is observed. Considering the average total leaf-deposited weight of 746.61 mg m^{-2}, the RMSE of network 1 (420.72 mg m^{-2}) still amounts 56%.

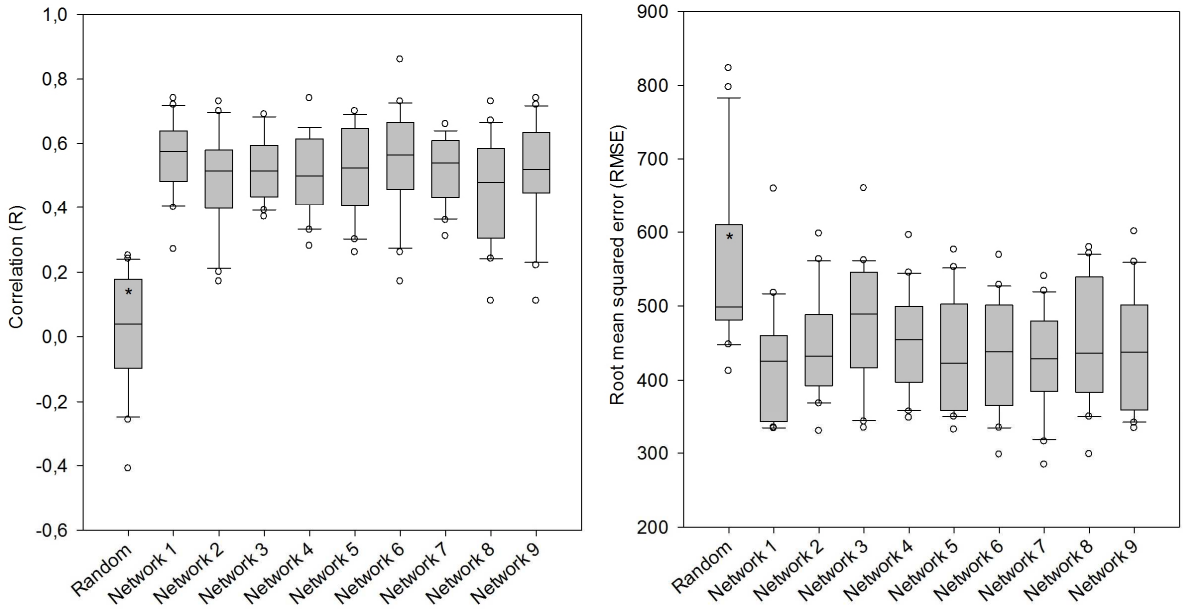

Figure 6: Boxplots of the correlations (left) and root mean squared errors in mg m^{-2} *(right) results of the different considered neural networks. Significant differences (p<0.05) are indicated by "*".*

Table 5: Correlation coefficient (R) between the measured and the modelled total weight and root mean square error (RMSE, mg m^{-2}*) results of the test data (n=38) after training of the considered neural networks (network 1-9) including a network based on random data (Random).*

	Random		**Network 1**		**Network 2**		**Network 3**		**Network 4**		**Network 5**		**Network 6**		**Network 7**		**Network 8**		**Network 9**	
Repetition	R	RMSE	R	RMSE	R	RMSE	R	RMSE	R	RMSE	R	RMSE	R	RMSE	R	RMSE	R	RMSE	R	RMSE
1	-0.09	486.04	0.40	445.27	0.43	418.31	0.60	411.07	0.44	439.53	0.44	503.30	0.45	493.64	0.54	471.98	0.35	496.36	0.74	357.90
2	-0.01	656.76	0.63	334.34	0.33	509.57	0.62	453.49	0.36	544.92	0.50	484.99	0.86	568.62	0.53	423.36	0.45	388.85	0.22	559.50
3	0.25	448.40	0.50	448.12	0.52	562.97	0.69	487.79	0.62	378.37	0.65	352.29	0.69	382.82	0.54	401.38	0.11	553.33	0.62	437.86
4	-0.41	823.00	0.63	339.35	0.51	381.18	0.42	660.23	0.39	440.26	0.50	472.86	0.49	417.31	0.44	451.25	0.24	450.27	0.50	454.07
5	0.02	619.28	0.72	352.42	0.43	464.73	0.48	500.51	0.33	595.59	0.40	500.46	0.64	334.09	0.64	382.38	0.56	434.64	0.58	410.80
6	0.21	412.25	0.54	510.12	0.54	494.45	0.37	553.84	0.65	442.21	0.64	412.38	0.68	423.33	0.58	434.44	0.25	563.02	0.67	359.67
7	-0.06	479.58	0.64	339.96	0.63	402.61	0.41	555.67	0.65	347.49	0.42	498.40	0.62	347.80	0.40	540.07	0.60	453.06	0.69	340.87
8	0.24	506.94	0.48	450.81	0.39	544.25	0.58	389.70	0.55	472.12	0.69	352.25	0.56	377.90	0.61	405.19	0.50	455.57	0.72	360.46
9	0.03	499.90	0.70	333.42	0.53	427.93	0.60	342.56	0.49	506.83	0.38	515.99	0.73	297.84	0.53	482.21	0.46	349.05	0.50	478.17
10	0.23	447.98	0.57	353.19	0.58	437.49	0.50	559.88	0.55	414.43	0.69	354.31	0.40	528.13	0.41	467.37	0.50	381.94	0.11	600.43
11	0.17	468.61	0.54	444.12	0.32	444.60	0.50	507.72	0.60	375.43	0.55	416.16	0.50	453.45	0.31	456.80	0.63	353.82	0.59	437.83
12	-0.26	797.05	0.67	335.32	0.57	329.70	0.55	362.64	0.40	537.76	0.32	552.39	0.67	364.48	0.60	393.01	0.59	393.00	0.47	480.18
13	0.05	558.19	0.64	412.85	0.70	390.14	0.53	459.79	0.47	504.23	0.53	406.15	0.56	467.70	0.63	381.47	0.45	388.17	0.52	552.93
14	0.08	494.88	0.27	659.53	0.17	470.90	0.69	333.91	0.63	357.03	0.63	412.38	0.48	456.36	0.61	315.46	0.57	430.59	0.44	502.93
15	0.18	497.66	0.58	463.04	0.66	377.23	0.43	490.44	0.55	467.34	0.69	349.02	0.60	453.45	0.66	284.11	0.29	579.19	0.54	420.36
16	-0.16	599.75	0.47	381.41	0.73	457.55	0.48	561.39	0.74	391.51	0.26	544.71	0.57	369.59	0.44	511.21	0.51	438.16	0.50	371.93
17	-0.10	583.34	0.74	390.48	0.42	425.57	0.39	507.85	0.51	475.38	0.70	331.79	0.45	514.13	0.36	520.40	0.38	554.87	0.52	353.27
18	0.17	493.65	0.49	517.33	0.20	597.37	0.55	434.17	0.28	485.81	0.59	372.51	0.26	503.82	0.64	345.56	0.26	570.55	0.37	543.59
19	0.11	493.34	0.59	465.32	0.58	400.57	0.45	520.45	0.44	425.74	0.30	575.60	0.65	336.40	0.58	406.83	0.73	298.17	0.64	333.55
20	-0.13	613.07	0.44	438.05	0.46	368.35	0.55	460.03	0.47	485.68	0.52	429.11	0.17	516.80	0.43	482.55	0.67	361.35	0.32	496.32
Average:	**0.03**	**548.98**	**0.56**	**420.72**	**0.49**	**445.27**	**0.52**	**477.66**	**0.51**	**454.38**	**0.52**	**441.85**	**0.55**	**430.38**	**0.52**	**427.85**	**0.46**	**444.70**	**0.51**	**442.63**

4. Conclusions

To our knowledge, the application of ground-based LiDAR for comparison with gravimetric results of leaf-deposited particulate matter is presented for the first time. Within this study, ground-based LiDAR has shown to be a very promising tool for fast and non-destructive acquisition of detailed three dimensional tree structure information. Translation of the LiDAR-derived point clouds into voxelized leaf area densities (LAD) might provide valuable information for urban air quality models, where tree crowns are most often represented very rudimentary.

Apart from physical effects like height, azimuth and tree position, this study evaluated the influence of tree crown morphology (leaf density) on the amount of leaf-deposited dust. Overall, we can say that the effect of leaf density appears limited. Increasing leaf density results in a decreasing leaf-deposited particle mass per unit leaf area, most strongly observed in the middle of the street canyon (NW and SE azimuth). As the experienced perpendicular wind flow will be influenced near the street canyon walls (NE and SW azimuth), greatest influence of leaf density on wind-induced particle deposition can be expected in the middle of the street canyon. A dense tree canopy might influence leaf-deposition of atmospheric particles through attenuation of the wind-induced impaction process. Apart from the aerodynamic effect of tree crown morphology (scenario 1), no effect of rain-induced particle wash-off can be observed (scenario 2). As no significant relation between leaf density and the leaf-deposited particle mass was observed in either the regression or neural network analyses and the observed effect of leaf density in the linear mixed-effects model approach only accounts for a 7% AIC decrease compared to the model with only physical effects, the leaf-deposited particle mass seems to be mainly determined by physical factors and to a much lesser extent by leaf density. We recognize that the effect of leaf density might be different for other tree species as it is a tree-specific characteristic. Comparison of multiple tree species with different structures might, therefore, be interesting for future research. Moreover, this study only focussed on the effect of leaf density on leaf-deposited particle mass and not on the local dispersion of PM polluted air which might be an important additional

effect of tree-crown morphology. Finally, only the surface-accumulated particles were quantified gravimetrically, while part of the leaf-deposited particles have shown to encapsulate inside epicuticular wax layers (Dzierzanowski et al. 2011, Terzaghi et al. 2013, Hofman et al. 2014a). Application of LiDAR-derived tree crowns in air quality models might shed more light on the influence of urban tree crown morphology on the local distribution of atmospheric particles and the resulting leaf-deposition.

Acknowledgements

We would like to thank Prof. Dr. Willy Maenhaut and Prof. Dr. Magda Claeys of the Department of Pharmaceutical Sciences of the University of Antwerp for the use of their laboratory and the support during the weighing procedure and the Flemish Environment Institute (VMM) for supplying the meteorological data. Moreover, we would also like to thank the city council services of the city of Antwerp and the residents of the "De Villegasstraat" for their support during the sampling campaign.

References

Beckett, K. P., P. H. Freer-Smith, and G. Taylor. 1998. Urban woodlands: their role in reducing the effects of particulate pollution. Environmental Pollution **99**:347-360.

Beckett, K. P., P. H. Freer-Smith, and G. Taylor. 2000. Particulate pollution capture by urban trees: effect of species and windspeed. Global Change Biology **6**:995-1003.

Calders, K., J. Armston, G. Newnham, M. Herold, and N. Goodwin. 2014. Implications of sensor configuration and topography on vertical plant profiles derived from terrestrial LiDAR. Agricultural and Forest Meteorology **194**:104-117.

Dzierzanowski, K., R. Popek, H. Gawrońska, A. Saebø, and S. W. Gawroński. 2011. Deposition of particulate matter of different size fractions on leaf surfaces and in waxes of urban forest species. International Journal of Phytoremediation **13**:1037-1046.

EEA. 2013. Air quality in Europe - 2013 report. European Environment Agency, Copenhagen, Denmark.

Èermák, J. 1998. Leaf distribution in large trees and stands of the floodplain forest in southern Moravia. Tree Physiology **18**:727-737.

Gromke, C. and B. Ruck. 2007. Influence of trees on the dispersion of pollutants in an urban street canyon - Experimental investigation of the flow and concentration field. Atmospheric Environment **41**:3287-3302.

Hagan, M. T. and M. B. Menhaj. 1994. Training feedforward networks with the Marquardt algorithm. Neural Networks, IEEE Transactions on **5**:989-993.

Hofman, J., I. Stokkaer, L. Snauwaert, and R. Samson. 2013. Spatial distribution assessment of particulate matter in an urban street canyon using biomagnetic leaf monitoring of tree crown deposited particles. Environmental Pollution **183**:123-132.

Hofman, J., K. Wuyts, S. Van Wittenberghe, M. Brackx, and R. Samson. 2014a. On the link between biomagnetic monitoring and leaf-deposited dust load of urban trees: Relationships and spatial variability of different particle size fractions. Environmental Pollution **189**:63-72.

Hofman, J., K. Wuyts, S. Van Wittenberghe, and R. Samson.2014b. On the temporal variation of leaf magnetic parameters: seasonal SIRM accumulation of leaf-deposited and leaf-encapsulated particles of a roadside tree crown. Science of The Total Environment **493**: 766-772.

Hosoi, F. and K. Omasa. 2006. Voxel-Based 3-D Modeling of Individual Trees for Estimating Leaf Area Density Using High-Resolution Portable Scanning Lidar. Geoscience and Remote Sensing, IEEE Transactions on **44**:3610-3618.

Hosoi, F. and K. Omasa. 2007. Factors contributing to accuracy in the estimation of the woody canopy leaf area density profile using 3D portable lidar imaging. Journal of Experimental Botany **58**:3463-3473.

Kardel, F., K. Wuyts, B. A. Maher, R. Hansard, and R. Samson. 2011. Leaf saturation isothermal remanent magnetization (SIRM) as a proxy for particulate matter monitoring: Inter-species differences and in-season variation. Atmospheric Environment **45**:5164-5171.

Langner, M. 2007. Reduction of airborne particulates by urban green. Page 138 *in* Economic Valuation of Biological Diversity – Ecosystem Services. German Federal Agency for Nature Conservation, Vilm.

Lee, K. W. and R. Mukund. 1993. Filter Collection. Pages 197-205 *in* W. K. and B. P.A., editors. Aerosol measurement: Principles, Techniques and applications. Van Norstrand Reinhold, New York.

Lera, G. and M. Pinzolas. 2002. Neighborhood based Levenberg-Marquardt algorithm for neural network training. Neural Networks, IEEE Transactions on **13**:1200-1203.

Litschke, T. and W. Kuttler. 2008. On the reduction of urban particle concentration by vegetation - a review. Meteorologische Zeitschrift **17**:229-240.

Lovell, J. L., D. L. B. Jupp, D. S. Culvenor, and N. C. Coops. 2003. Using airborne and ground-based ranging lidar to measure canopy structure in Australian forests. Canadian Journal of Remote Sensing **29**:607-622.

Maher, B. A., I. A. M. Ahmed, B. Davison, V. Karloukovski, and R. Clarke. 2013. Impact of Roadside Tree Lines on Indoor Concentrations of Traffic-Derived Particulate Matter. Environ Sci Technol **47**:13737-13744.

MathWorks Inc. . 2013. Matlab 8.1. MathWorks Inc., Natick, US.

Matzka, J. and B. A. Maher. 1999. Magnetic biomonitoring of roadside tree leaves: identification of spatial and temporal variations in vehicle-derived particulates. Atmospheric Environment **33**:4565-4569.

Mitchell, R., B. A. Maher, and R. Kinnersley. 2010. Rates of particulate pollution deposition onto leaf surfaces: Temporal and inter-species magnetic analyses. Environmental Pollution **158**:1472-1478.

Pinheiro, J., D. Bates, S. DebRoy, D. Sarkar, and R Development Core Team. 2012. nlme: Linear and Nonlinear Mixed Effects Models. Pages R package version 3.1-105.

R Core Team. 2012. R: A Language and Environment for Statistical Computing. R Foundation for Statistical Computing, Vienna, Austria.

Ruijgrok, W., H. Tieben, and P. Eisinga. 1997. The dry deposition of particles to a forest canopy: A comparison of model and experimental results. Atmospheric Environment **31**:399-415.

Sæbø, A., R. Popek, B. Nawrot, H. M. Hanslin, H. Gawronska, and S. W. Gawronski. 2012. Plant species differences in particulate matter accumulation on leaf surfaces. Science of The Total Environment **427–428**:347-354.

SGS. 2010. Strategische geluidsbelastingskaarten agglomeratie Antwerpen. 090357-2-v1, SGS Belgium NV.

Steffens, J. T., Y. J. Wang, and K. M. Zhang. 2012. Exploration of effects of a vegetation barrier on particle size distributions in a near-road environment. Atmospheric Environment **50**:120-128.

Szönyi, M., L. Sagnotti, and A. M. Hirt. 2008. A refined biomonitoring study of airborne particulate matter pollution in Rome, with magnetic measurements on Quercus Ilex tree leaves. Geophysical Journal International **173**:127-141.

Terzaghi, E., E. Wild, G. Zacchello, B. E. L. Cerabolini, K. C. Jones, and A. Di Guardo. 2013. Forest Filter Effect: Role of leaves in capturing/releasing air particulate matter and its associated PAHs. Atmospheric Environment **74**:378-384.

Urbat, M., E. Lehndorff, and L. Schwark. 2004. Biomonitoring of air quality in the Cologne conurbation using pine needles as a passive sampler—Part I: magnetic properties. Atmospheric Environment **38**:3781-3792.

Van der Zande, D. 2008. Mathematical Modeling of 3D canopy structure in forest stands using ground-based LIDAR. K.U.Leuven, Leuven.

Vardoulakis, S., B. E. A. Fisher, K. Pericleous, and N. Gonzalez-Flesca. 2003. Modelling air quality in street canyons: a review. Atmospheric Environment **37**:155-182.

Vos, P. E. J., B. Maiheu, J. Vankerkom, and S. Janssen. 2013. Improving local air quality in cities: To tree or not to tree? Environmental Pollution **183**:113-122.

Wang, H., G. Xing, and K. Chen. 2008. Categorical Data Transformation Methods for Neural Networks. Pages 262-266 *in* Conference on Information and Knowledge Engineering.

WHO. 2006. Air quality guidelines for particulate matter, ozone, nitrogen dioxide and sulfur dioxide. Global update 2005. World Health Organization, Copenhagen.

WHO. 2010. Hidden cities: Unmasking and overcoming health inequities in urban settings., World Health Organisation, Centre for Health Development (WHO Kobe Center) and United Nations Human Settlements Program (UN-HABITAT).

WHO. 2014. Fact Sheet: Ambient (outdoor) air quality and health. WHO Media Centre.

Yang, J., J. McBride, J. Zhou, and Z. Sun. 2005. The urban forest in Beijing and its role in air pollution reduction. Urban Forestry & Urban Greening **3**:65-78.

Zande, D. V. d., I. Jonckheere, J. Stuckens, W. W. Verstraeten, and P. Coppin. 2008. Sampling design of ground-based lidar measurements of forest canopy structure and its effect on shadowing. Canadian Journal of Remote Sensing **34**:526-538.

Zhang, C., B. Huang, Z. Li, and H. Liu. 2006. Magnetic properties of high-road-side pine tree leaves in Beijing and their environmental significance. Chinese Science Bulletin **51**:3041-3052.